Residual stress evaluation of adhesively bonded composite using central cut plies specimens

Baldassarre, Alessandro; Martinez, Marcias; Rans, Calvin

DOI
10.1080/00218464.2019.1598862

Publication date
2020

Document Version
Accepted author manuscript

Published in
Journal of Adhesion

RESIDUAL STRESS EVALUATION OF ADHESIVELY BONDED COMPOSITE USING CENTRAL CUT PLIES SPECIMENS

Alessandro Baldassarre[1,a], *Marcias Martinez*[1,2,b], *Calvin Rans*[2,c]

[1] Department of Mechanical and Aeronautical Engineering, Clarkson University, 8 Clarkson Ave, Potsdam, NY 13699

[2] Faculty of Aerospace Engineering, Delft University of Technology, Building 62, Kluyverweg 1, 2629 HS Delft

[a] baldaa@clarkson.edu, [b] mmartine@clarkson.edu, [c] C.D.Rans@tudelft.nl

Keywords: Bonded Composite Joints and Repairs, Residual Stresses, Strains Monitoring, Central Cut Plies Specimen, Embedded Optical Fiber, Distributed Sensing System.

Abstract

The present study reports on the evaluation of residual stress field formation and distribution in Central Cut Plies (CCP) specimens. Real-time measurements were performed using a distributed sensing fiber optic system based on Rayleigh Backscattering, which was successfully able to capture strain distribution inside the adhesive layer at every 0.65 mm during the entire curing cycle, for both unidirectional and cross ply laminate configurations. A finite element analysis was also performed to cross-correlate with the experimental residual strain distributions in the proximity of the severed central cut plies. The results outlined in this study demonstrate the presences of tensile residual stresses within the adhesive layer for both configurations. A full field strain distribution and the significance of these findings in relation to the use of the CCP test for

fracture mechanics testing will be discussed. Results of this study have shown that residual stresses arise after the curing process for which the amount of longitudinal and transverse residual stresses for the unidirectional CCP laminate are 61% and 19% of the total strength of the adhesive respectively, while for the cross-ply CCP laminate are 72% and 71%, respectively.

Introduction

The increasing demand for high-strength and low-weight structures in the aeronautical industry, in addition to the emission reduction policies motivated by the civil aviation organization [1], has led to an increase in the use of composite materials. These materials, however, generally have a more complex failure behavior characterized by the presence and interaction of multiple failure mechanisms such as fibre-matrix debonding, delamination, and matrix cracking. Developing an in-depth understanding of these failure modes has been an area of concentrated effort by the research community, particularly in terms of developing predictive capabilities for design [2] [3] [4] [5].

Currently, 50% of the aircraft structures, such as the Boing 747 series, employ the use of fasteners for the assembling of primary and secondary structure [6], while repairs that employ a combination of mechanical fasteners and adhesive are regulated by specific certification requirements [7] [8]. The application of rivets, pins or blind fasteners have an impact on the overall weight of the structure, in addition to creating high stress concentration regions in the structure that could lead to the formation of disbond sites [9].

Nowadays, adhesive bonding is becoming a prominent alternative due to their low-weight impact and fatigue-resistance, providing the same strength as rivets and fasteners [1]. However, one of the primary challenges that the bonded joint community faces is the presences of kissing bonds or zero volume bonds. These types of defects are primarily caused by poor adhesion of two surfaces bonded together, preventing the joint from carrying the loads. Although there are advantages to purely bonded joints, it has also been shown that both bonded joints and bonded repairs have unexpectedly failed under adhesive bond failure due to in-service loads [10]. Investigations on the F-111, from The Royal Australian Air Force (RAAF), have shown that failure in adhesive bonds has led to extensive damage on components or structure in 53% of the cases [10].

All the adhesively bonded structure/components that undergo curing cycle are exposed to residual stress formations due to the mismatch between the Coefficient of Thermal Expansion (CTE) of the adhesive and the carbon fiber layers. These residual stresses are intrinsic forces within each lamina generated after the cooling phase [11]. As such, both carbon/epoxy and adhesive layers undergo strength degradation. This is particularly true for the subject of joining and repairing, as the adhesive layer typically represent a critical weak point in any structure. In addition, the evaluation of residual stresses in adhesively bonded structures is crucial for understanding their effect on mode II disbonding propagation under fatigue cycles.

Many authors have addressed the effect of residual strains in adhesively bonded composite. Some of the authors investigated the determination of residual stresses on bonded repairs [12] [13] [14], while others investigated residual stresses in composite bonded joints [15] [16] [17]. Daverschot et al. addressed the issue of thermal residual stresses in bonded composite repairs

by comparing the analytical solution with a numerical model. They considered GLARE-2 and boron/epoxy bonded to an aluminum 2024-T3 using FM-73 adhesive. They investigated the accuracy of the Wang-Rose model and the van Barneveld-Fredell model with respect to FE analysis of two different types of specimen. The first test specimen consisted of a repair patch freely allowed to expand while the second specimen consisted of a realistic repair in which the expansion of the patch was constrained. For the GLARE patch, the study showed tensile residual stresses for the test specimen and compressive residual stresses for the in-field specimen. For the boron/epoxy patch, tensile residual stresses were observed for both types of specimens [12]. Albat et al. investigated thermal residual stresses of a unidirectional boron/epoxy laminate adhesively bonded to a cracked aluminum plate with FM-73 epoxy adhesive. Compressive and tensile residual stresses were measured within the boron/epoxy patch and at the interface between the aluminum and the adhesive [13]. However, none of the aforementioned studies considered the effect of residual stresses in the adhesive layer. Only a few papers in the literature considered residual strain measurements in the adhesive layer for metal-composite or composite-composite structure [18] [19] [17]. Aminallah et al. and Mhamdia et al. investigated the residual stress distribution in repaired aluminum plates by using boron/epoxy composite patch and FM-73 adhesive bonding through a Finite Element Method (FEM). In both cases, tensile residual stresses and compressive residual stresses were found in the aluminum plate and the composite patch, respectively. In the adhesive layer in-plane shear residual stresses were found to be higher at the interface perimeter between the patch and the plate, which can play an important role on the formation of a disbond, while negligible everywhere inside the adhesive [18] [19]. In both studies, no mention was made whether stresses along and transverse to the

fiber direction within the adhesive layer were negligible. Schoeppner et al. analyzed residual stresses in composite bonded joints. Residual strains were measured using the Moire' Interferometer Technique and converted into residual stresses through an in-house linear stress analysis program. The linear analysis-based software prediction resulted in an overestimation of the residual stresses due to high strain variability within the plies [17].

In order to obtain certifications from the authorities on pure bonded joints, a better understating on the disbond propagation under fatigue loading is needed. It has been proven that disbond of mode II is the primary cause of crack growth in adhesively bonded joints [20] [21]. For this reason, Central Cut Ply (CCP) specimen, which schematic is shown in Figure 2, has been considered by many authors for understanding the fracture mechanics of mode II [22] [23] [24]. This type of configuration has been chosen as a replacement to other specimen types such as the End Notched Flexure (ENF), the End Loaded Split (ELS), and the four points End Notched Flexure (4ENF), as described in [25] [26] [27] [28] [29]. The primary advantage of the CCP specimen is the measurement of the fracture toughness independent of the crack length. In fact, one of the most challenging part in the ENF, ELS, and 4ENF tests is the measurement of the crack length at any given load, in addition to the frictional effects and instability of crack propagation. All these drawbacks were overcome by using the CCP configuration.

The use of CCP specimens for the understanding of residual stresses is hypothesized to provide a better insight on the interaction between the disbond growth rate and residual stress fields. As such, the primary objective of the current study is to determine the presence of residual stresses and their corresponding magnitude in a CCP specimen with different layup sequence through both experimental and FE methods.

Methodology

In order to investigate the possible presence of residual stresses in a typical fracture mechanics specimen used for characterizing disbond growth resistance and/or acceleration, an experimental and numerical approach through the use of the Distributed Sensing System (DSS) and Ansys Workbench™ respectively, was considered in unidirectional and cross-ply carbon/epoxy CCP laminates. The paper focused on the residual strains within the adhesive layer while residual strains within the carbon fiber layers were not part of this investigation.

The current section outlines the mechanical and thermal properties obtained for the carbon/epoxy prepreg used in this study, including the laminate configuration, the method used to estimate the residual strains accounting the effect of the embedded optical fiber, and the Finite Element model created for the numerical analysis.

Material characterization

Prior to investigating the behavior of the CCP fracture mechanics specimen, the material properties of the composite prepreg material and adhesive material to be used within this study needed to be evaluated. The material chosen for this study is a unidirectional carbon-epoxy prepreg material DA 4518U and an epoxy film adhesive DA 4518 with a nylon carrier fabric produced by Adhesive Prepregs Composite Manufacturers (APCM) (Plainfield, CT (USA)) [30].

The properties were particularly necessary as inputs for the FE analysis performed to validate the experimental results.

The mechanical properties of the carbon fiber-epoxy resin prepregs, employed in this study, were evaluated following ASTM standards: D3039/D3039M [31], D7291/D7291M [32], and D5379/D5379M [33] for the in-plane elastic modulus, through-thickness elastic modulus and the shear properties, respectively. The material properties for the epoxy resin, instead, were determined through the ASTM standards D638 [34]. An epoxy-resin laminate of 24 layers (for a total thickness of 3.6 mm) was manufactured following the curing cycle shown in Figure 4. The laminate was cut into six dog-bone shape specimens.

Although the ASTM standards recommend the use of foil gauges, the authors instrumented each coupon with a fiber optic Distributed Sensing System from Luna Inc. (Roanoke, VA (USA)) [35], Digital Image Correlation from Correlated Solution (Irmo, SC(USA)) [36], in addition to strain gauges from HBM (Marlborough, MA (USA)) [37]. The values obtained from the DSS and DIC were found to be within 10% of error with respect the strain gauges. A summary of the mechanical and thermal properties are shown in Table 1.

Table 1. Material properties for DA 4518U and DA4518.

Material	***Property***	***Value***	***Unit***
Carbon/epoxy UD DA4518U	Density, ρ	1.43	$\frac{\mathrm{g}}{\mathrm{cm}^3}$
	Elastic modulus, E_{xx}	104	GPa
	Elastic modulus, E_{zz}	7	GPa
	Major Poisson's ratio, ν_{xz}	0.28	-
	Shear modulus, E_{xz}	4	GPa
	Tensile strength, σ_{xx}^{TS}	1300	MPa
Adhesive (epoxy resin) DA4518	Density, ρ	1.11	$\frac{\mathrm{g}}{\mathrm{cm}^3}$
	Elastic modulus, E	1.76	GPa
	Poisson's ratio, ν	0.28	-
	Tensile strength, σ^{TS}	14.3	MPa

Measuring the Coefficient of Thermal Expansion (CTE) of the carbon fiber and resin is crucial for determining the amount of residual strain/stress formed during the curing process. Standard procedures, such as ASTM E831, ASTM D696, and ISO 11359, require either a Thermo-Mechanical Analysis (TMA) or a dilatometer for measuring the expansion/contraction rate as function of temperature. In this study, thermal properties were obtained using an optical fiber connected to a DSS which has been successfully employed by other authors for measuring CTE of aluminum, steel, fiberglass, and carbon fiber [38] [39] [40] [41]. An Optical Distributed Sensor Interrogator (ODiSI) from LUNA Technology was employed for strain and temperature measurements [35]. The system is based on the Rayleigh backscattering principle in which the light is back-reflected due to perturbations on the optical fiber. The sensor configuration, the analysis, and the post-processing were performed with ODISI-B v5.2.2.

Two methods were chosen to obtain the CTE of the carbon fiber. Luna Inc. suggest a “single fiber loop” or a “point-to-point compensation” experiment for compensating temperature gradients on mechanical strain measurements [42].

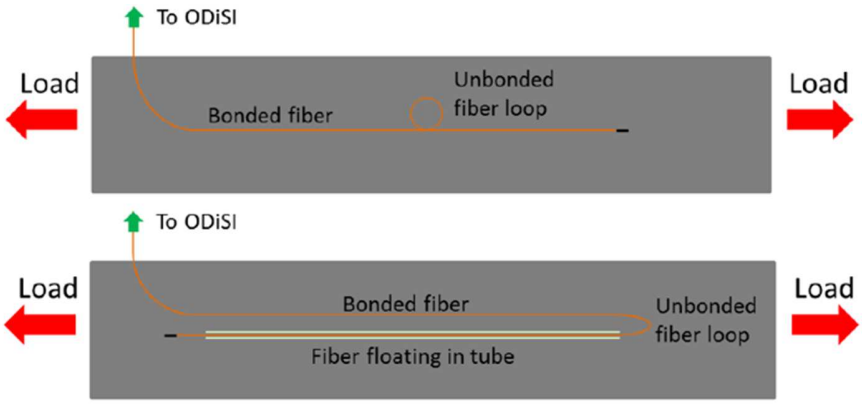

Figure 1. Temperature compensation for measuring spectral shift with the ODISI-B system.

The single fiber loop set-up was chosen for this purpose, where the un-bonded fiber is used to compensate for the mechanical strains (ε_{L_i}) as described in the following equation:

$$\varepsilon_{L_i} = \left(\Delta\upsilon_{B_i} * k_\varepsilon\right) - \left((k_{nT} * \Delta\upsilon_U * k_\varepsilon) + (\Delta\upsilon_U * k_T * \alpha_s)\right) \quad (1)$$

Where k_{nT} is the thermal response of the fiber, α_s is the CTE of the structure, k_ε and k_T are the strain conversion factor and the temperature conversion factor respectively, $\Delta\upsilon_U$ is the spectral shift in the un-bonded fiber, and $\Delta\upsilon_{B_i}$ is the spectral shift in the bonded fiber. The CTE of the material can be obtained by Equation 2, ensuring no mechanical constraints during the curing process ($\varepsilon_{L_i} = 0$):

$$\alpha_s = \frac{\left(\Delta\upsilon_{B_i} * k_\varepsilon\right) - (k_{nT} * \Delta\upsilon_U * k_\varepsilon)}{(\Delta\upsilon_U * k_T)} \quad (2)$$

For most germanosilicate core fibers, the temperature and strain conversion factors are $k_\varepsilon = -6.67^o \frac{\mu\varepsilon}{GHz}$ and $k_T = -0.801^o \frac{C}{GHz}$, respectively, while k_{nT} is approximately 0.95 [42]. The value of the spectral shift in the un-bonded fiber and in the bonded fiber was recorded at both $60^o C$

and 80^oC. The $\Delta\upsilon_U$ and $\Delta\upsilon_{B_i}$ values employed in equation 2 are the difference of spectral shift at the two referenced temperature [42].

To obtain confidence and verify the process, 6000 series aluminum alloy specimens were tested. Its Elastic modulus of 68.9 GPa and a Poisson's ratio of 0.33 were validated by the author through tensile testing. The CTE for 6000 series aluminum alloys, varies from 23.4 $\frac{ppm}{^oC}$ and 23.6 $\frac{ppm}{^oC}$ for Al6063-T6 [43] and Al6061-T6 [44], respectively. The assessed value of the CTE for the specimens was found to be 23.4 $\frac{ppm}{^oC}$. The same procedure was then employed for evaluating the longitudinal and transverse CTE for the carbon fiber prepregs as well as the adhesive. The thermal properties of the DA 4518U carbon epoxy system was found to be $-0.3\ ppm/^oC$ and $42\ ppm/^oC$ for longitudinal and transverse CTE, respectively. The DA4518 epoxy system, comprised of the carrier, showed a CTE of $42.9\ ppm/^oC$.

CCP specimen test

Production and configuration

The CCP specimens consists of a series of cut-layers sandwiched in between continuous layers, as shown in Figure 2. For the purpose of this study, the continuous plies are bonded to the cut plies through an adhesive layer. The laminates have symmetric layup sequence to avoid warping, with dimensions of 153 mm x 153 mm x 2.22 mm (LxWxT) while the distance between the cut plies was set to $5\ mm$ for all the experimental tests. The chosen layup sequence for unidirectional was $[0_4, adhesive, 0_{2cut}]_s$ while $[0, 90_2, 0, adhesive, 0_{2cut}]_s$ for the cross-ply configuration.

In this study, all laminates were manufactured considering a secondary bonding technique in which two independent curing cycles were employed during the CCP laminate production. The

first curing cycle ensured preparation of each laminate (i.e. two continuous fiber laminates and two cut fiber laminates using DA4518U prepreg only), while the second curing cycle ensured bonding of the individual laminates into a single specimen (using both DA4518U and DA4518 prepreg), conforming the CCP laminates, as shown in Figure 2. According to the manufacturer, both types of prepregs follow the same curing cycle (press cure for 1 hour at 121^oC) [45] [46]. Therefore, the first curing cycle is the same as the second curing cycle, shown in Figure 4.

In a prior step, a co-curing method was employed for residual strains determination. However, a co-curing process led to inaccurate results. These inaccuracies were believed to come from the shifting of the embedded fiber into the adjacent carbon fiber layer during the curing process. Therefore, the value of residual strains captured by the sensor were related to the carbon fiber layer and not to strains produced at the adhesive layer. This challenge was resolved by using a secondary bonding technique in which the carbon fiber laminates were already cured at an earlier stage and therefore, avoid the penetration of the fiber into the neighboring layers.

Table 2. Summary of the experimental tests.

CCP laminate configuration	**# of test**	**Curing cycle**	**Lay-up Sequence**	**Pre-pregs[1]**
Unidirectional	3	One dwell at 121^oC	$[0_4, adhesive, 0_{2cut}]_s$	DA 4518U (carbon fiber) DA 4518 (adhesive)
Cross-ply	3	One dwell at 121^oC	$[0, 90_2, 0, adhesive, 0_{2cut}]_s$	DA 4518U (carbon fiber) DA 4518 (adhesive)

[1] The prepregs were from Adhesive Prepregs Composite Manufacturers [30]

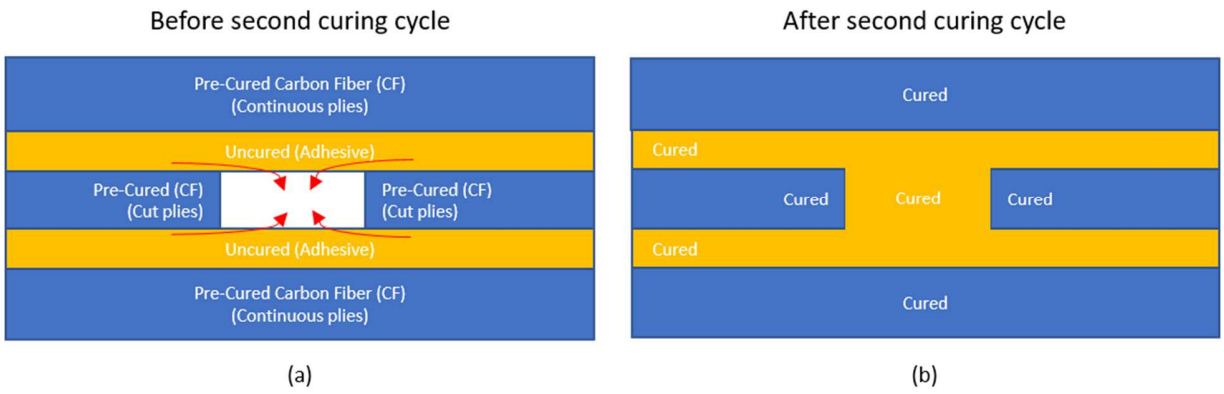

Figure 2. Secondary Bonding Configuration of the Central Cut Ply Laminate: (a) before the second curing cycle and (b) after the second curing cycle.

Instrumentation

An optical fiber was embedded inside the CCP laminate during the manufacturing process in order to record strains throughout the entire curing process. The first section of the optical fiber was embedded within the upper adhesive layer longitudinally while the second section was embedded within the lower adhesive layer transversally at $1\ mm$ from the adhesive gap, as shown in Figure 3. The optical fiber was placed along the carbon fiber direction between the adhesive layer and the cut plies at the bottom side, with respect to the central plane of the laminate. In the same manner, the fiber was embedded transverse to the carbon fiber in the upper sections of the CCP specimen. The schematic representation of the embedded optical fiber is shown in Figure 3. Once the fiber is placed within a laminate, the authors recorded specific sections along the length of the fiber by pressing on it. This creates a temporary strain increment at that point, which the authors are able to document prior to curing the laminate. The accuracy of the selected point on the optical fiber is within a ±1.3 mm. This determines which portions of the fiber are embedded along or transverse to direction of the layup sequence. Although the use of fiber optic system proved to be successful in capturing in real time the residual strain fields

during the curing process, it was evident that the use of a continuous fiber that spans along both the longitudinal and transverse direction was not an efficient means of capturing both strain fields simultaneously. One challenge encountered during this study was obtaining a clear strain measurement after the application of vacuum $(1\ bar)$, which affected the second section of the embedded fiber. In our case, the first section of the embedded fiber was always monitoring the longitudinal strains since a clear signal was needed to capture the strain distribution in all the three regions of the CCP laminate. The second section of the embedded fiber, was used to monitor the transverse strains which were constant throughout the entire width of the CCP laminate and therefore, not susceptible to significant error due to the applied vacuum.

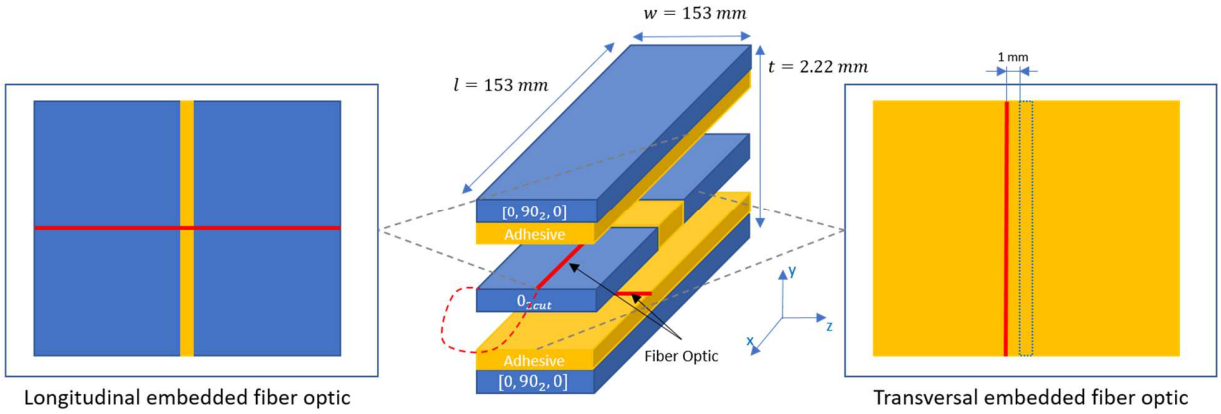

Figure 3. Schematic representation of the embedded optical fiber inside the CCP laminate.

The adhesive gap is unfilled prior to curing, as shown in Figure 2(a). During the curing process the resin starts to flow inside the gap due to a reduction in viscosity of the resin in addition to the applied vacuum. The gap is thus filled with resin without the presence of a carrier. Therefore, while the mechanical properties of the adhesive layers were the same as the ones outlined in

Table 1, the material properties of the resin along the adhesive gap were determined through the rule of mixture, shown in equation 3:

$$E_{adh} = E_r * v_r + E_n * v_n \quad (3)$$

where E_{adh}, E_r, and E_n are the Elastic modulus of the adhesive (provided by the manufacturer which comprised the nylon carrier within the epoxy resin), modulus of the resin, and modulus of the nylon carrier, while v_r and v_n represent the fiber volume fraction of the resin and the nylon, respectively. Since the DA4518 is a type of prepreg that comprises both epoxy resin and nylon carrier, the authors assumed the epoxy system as "composite" in which the nylon behaves as reinforcement surrounded by the epoxy resin. This allowed the authors to compute the elastic modulus of the only resin through the rule of mixture. According to the manufacturer, the resin content of the epoxy prepreg system DA 4518 varies between 45% and 50% by weight [30]. The averaged resin content was chosen to be 48% which provides a 52% nylon content. The most common commercial nylon is Nylon 6/6 which has an Elastic modulus of $2.93\ GPa$ and a density of $1.15\ \frac{g}{cm^3}$, under dry condition [47] while the density of the resin was determined by solving the volume fraction equation shown in equation 4:

$$\rho_r = \frac{\rho_n}{\frac{2\rho_n}{\rho_{adh}} - 1} \quad (4)$$

where ρ_{adh}, ρ_r, and ρ_n is the density of the adhesive layer, the epoxy resin, and the nylon carrier, respectively. The volume fraction of each constituent was obtained from the ratio between the weight and the density of the respective materials. The elastic modulus of the resin was computed from the rule of mixture outlined in equation 5:

$$E_r = \frac{E_{adh} - E_n * v_n}{v_r} \quad (5)$$

Finally, the Elastic modulus of the resin within the adhesive gap of the CCP laminate was found to be $0.493\ GPa$.

Measurements

Strain values within the adhesive layer were captured by the fiber optic at the end of the curing cycle as the sum of all the three types of strains. The decoupling of these terms was performed by post-processing the data captured with the DSS. The chosen mode of operation of the ODISI-B system allowing strain measurements every 1.3 mm (gage length) at a data acquisition rate of 23.8 Hz. However, the system averages the strains along the optical fiber every 0.65 mm (gage pitch) with an accuracy of approximately ±40με. The maximum and minimum range of strains and temperature allowed by the system is ±10,000 με and $-40^oC/220^oC$. Strain measurements were recorded, in the form of "scans", every $0.1\ Hz$ (10 seconds). Each point in Figure 4 was estimated through the ODISI-B post processing software by considering the time step of the actual curing cycle which corresponds to a specific scan value.

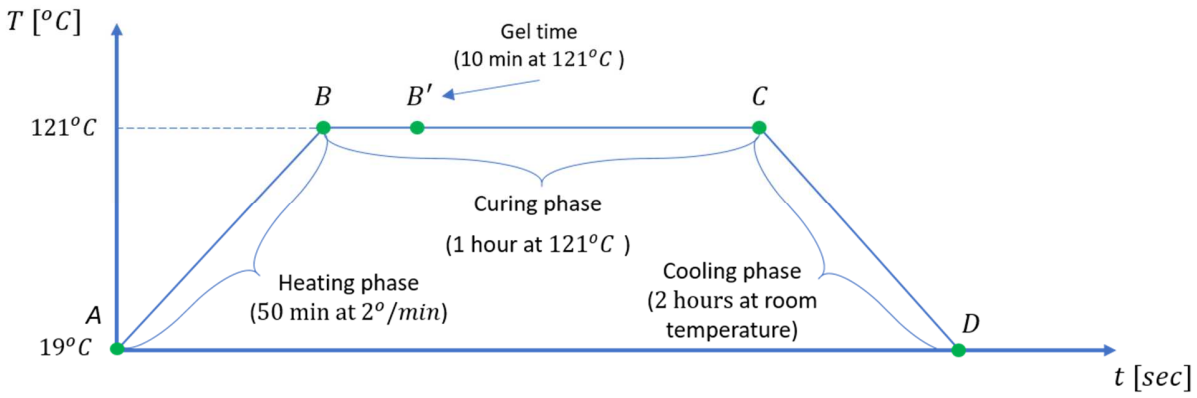

Figure 4. Phases of the curing cycle.

The curing cycle was provided by the APCM manufacturer for both DA4518 and DA4518U [45] [46]. Both prepregs are designed to cure at 121^oC (250^oF) and 177^oC (350^oF). The tests were performed using the 121^oC curing temperature. As shown in Figure 4, the curing cycle is comprised of three main phases: heating, curing, and cooling phase. Each of the three phases of the curing cycle introduces thermal, chemical, and residual strain, respectively. In the heating phase ($\overline{AB}$) the temperature arises from room temperature to the curing temperature developing thermal strains due to the thermal expansion of adhesive layers and the optical fiber. The polyimide fiber used for this study was an Anhydrous Silica (ASITM) single mode fiber which comprised of a silica core, a silica cladding, and a polyimide coating with a diameter of 9.0±0.5, 125+1/-3, and 145±5, respectively. During the curing phase ($\overline{BB'} + \overline{B'C}$), after reaching the glass transition temperature (B'), the resin starts polymerizing introducing chemical strains in the adhesive layer, as all other parts of the specimen have been pre-cured. During the cooling phase ($\overline{CD}$) the laminate experiences an opposite ΔT (but same magnitude) compared to the heating phase, however in this stage the layers are all bonded together. In this phase, the thermal

expansion of each layer generates a lamina-lamina interaction developing residual strain fields within the materials. For the entire curing cycle, the total amount of strains can be expressed as follow:

$$\overline{AD} \rightarrow \varepsilon_{tot} = \varepsilon_{adh_{th}} - \varepsilon_{of_{th\_\overline{AB}}} + \varepsilon_{ch} + \varepsilon_{rs} + \varepsilon_{of_{th\_\overline{CD}}} \quad (6)$$

Where ε_{adh_th} are the thermal strain in the adhesive layer, $\varepsilon_{of_{th\_\overline{AB}}}$ (positive strain due to fiber expansion) and $\varepsilon_{of_{th\_\overline{CD}}}$ (negative strain due to fiber contraction) are the thermal strains arising from the heating and cooling for the optical fiber, respectively, ε_{ch} are the chemical strains, ε_{rs} are the residual strains formed after the curing process, while ε_{tot} are the total strains measured by the optical fiber.

To be able to compute the residual strains at the end of the cooling cycle, equation 6 is re-arranged in order to determine the residual strains in the adhesive of the CCP laminate as shown in equation 7:

$$\varepsilon_{rs} = \varepsilon_{tot} - \varepsilon_{adh_{th}} + \varepsilon_{of_{th_{\overline{AB}}}} - \varepsilon_{ch} - \varepsilon_{of_{th\_\overline{CD}}} \quad (7)$$

Each of the terms in equation 7, corresponds to a specific segment of the curing cycle described in Figure 4 as shown in equation 8.

$$\begin{gathered} \overline{AB'} \rightarrow \varepsilon_{adh_{th}} - \varepsilon_{of_{th}} \\ \overline{B'C} \rightarrow \varepsilon_{ch} \\ \overline{CD} \rightarrow \varepsilon_{rs} + \varepsilon_{of_{th}} \end{gathered} \quad (8)$$

The glass transition temperature (i.e. when resin starts polymerizing) occurs after ten minutes upon having reached the curing phase, also known as the gel time of the resin (specified by the

manufacturer), $\overline{AB} = \overline{AB'}$ which means there are no additional strains arising in the $\overline{BB'}$ segment. In the DSS post-processing software, the recorded strains were zeroed at the end of the heating phase, at the gel point, and at the end of the curing phase in order to capture thermal, chemical, and residual strains, respectively. The zeroing of the strains at point (B') allowed the authors to determine the chemical strains after the curing phase (point C). In the same manner, residual strains were recorded at the end of the cooling phase (D) in order to obtain the residual strains.

As shown in equation 7, additional strains are introduced into the total strains due to the thermal expansion of the polyimide fiber. Considering that the CTE of the polyimide fiber is approximately $10\frac{ppm}{^\circ C}$, an increment of temperature of 102^oC produced during the heating process, generates an additional 1020 με on the fiber. However, this strain is dependent on the ability of the fiber to expand or contract with respect to the adhesive layer. During the heating up phase all laminae and fiber segments are free to expand or contract. However, after resin polymerization, all laminae and fiber are constrained to one another. Therefore, during the cooling process, the fiber is no longer free to contract to the initial condition. Considering the aforementioned phenomenon and the procedure employed to isolate the strains terms, the amount of additional strain sensed by the fiber system (1020 με) must be removed from the measured total strains. The value of 1020 με is configuration dependent. Figure 5 shows a schematic of the lamina-lamina interaction during the cooling process between carbon fiber and adhesive for the unidirectional and cross-ply configuration. In the case of the cross-ply CCP laminate, at the end of the heating phase $\varepsilon_{of_{th\_\overline{AB}}} = 1020$ με for both longitudinal and transverse strains, since the

embedded optical fiber is free to expand. However, at the end of the cooling phase $\varepsilon_{of_{th\_\overline{CD}}} = 0$ as the resin has polymerized preventing the fiber from returning back to its original dimension. Thus, the additional $1020\ \mu\varepsilon$ thermal strains captured after the heating phase, must be subtracted from the measured total longitudinal and transverse strains.

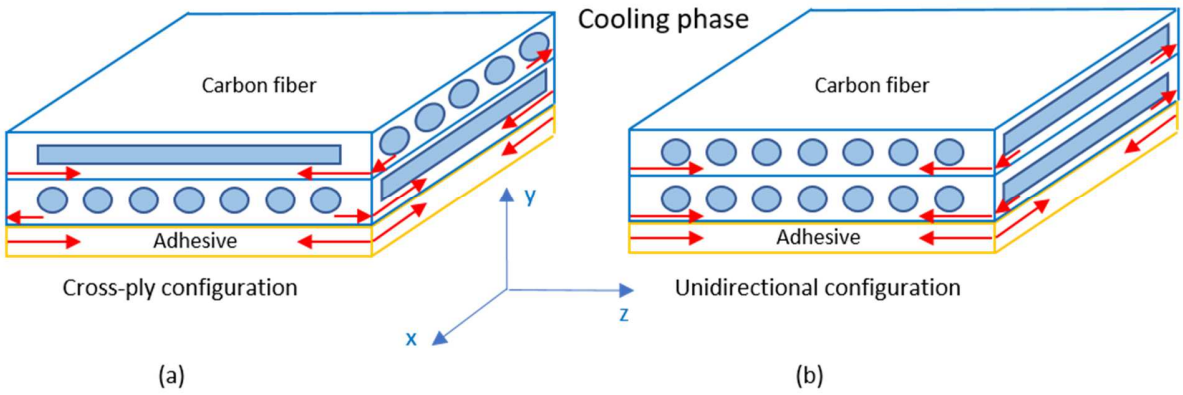

Figure 5. Expansion and contraction of each lamina during the cooling phase: (a) cross-ply and (b) unidirectional CCP laminate.

In case of the unidirectional CCP laminate, while $\varepsilon_{of_{th\_\overline{AB}}}$ is the same as for the cross-ply case, a distinction for $\varepsilon_{of_{th\_\overline{CD}}}$ must account that the longitudinal and transverse strain are different in a unidirectional laminate. For the longitudinal strains $\varepsilon_{of_{th\_\overline{CD}}} = 0$ since the adhesive is constrained to the carbon fiber layer, which do not exhibit significant deformation due to their small longitudinal CTE ($\alpha_{x_{CF}} = -0.3\ ppm/^oC$). For the transverse strains, instead, $\varepsilon_{of_{th\_\overline{CD}}} = -1020\ \mu\varepsilon$ because the adhesive layer (as well as the optical fiber) experience the same contraction as the carbon fiber layers which has a much higher transverse CTE ($\alpha_{z_{CF}} = 42\ ppm/^oC$). As can be noticed from equation 7, due to the non-zero nature of $\varepsilon_{of_{th\_\overline{CD}}}$ (-1020

με), the amount of additional strains that must be removed from the transverse total strains are twice the ones accounted for the longitudinal strains (-2040 με).

Finite Element Model

A finite element model of the CCP specimen was developed in order to validate the magnitude and nature of the residual strains measured in the CCP test specimens. The cooling process was simulated by applying a negative thermal loading which reproduced the expansion and contraction of the materials that occurs during curing but does not explicitly simulate cure kinetics. This procedure allowed the authors to correlate strain and stress distributions within the adhesive layer to the obtained experimental results.

Ansys Workbench™ was used to create a FEM for the unidirectional and cross-ply CCP laminate. The 0^o (longitudinal) and 90^o (transverse) plies were modeled along the x-direction and z-direction, respectively. The total dimensions of the panels were set to 153 x 153 x 2.22 mm matching those of the experiment with an adhesive gap size set to $5\ mm$. Each layer was modeled as a solid body to evaluate also the out of plane strains/stresses. Thermal loading ($\Delta T = -104^o C$) was applied to all laminate bodies to simulate temperature effect during the cooling process. Non-linear contact and geometry non-linearity were used during the analysis which generated convergence issue. For this reason, the thermal loading was applied in four steps, each step consisting in a $\Delta T = -26^o C$.

A prescribed set of boundary conditions which allowed for free expansion and shrinkage of the laminate with no rotations, was considered as shown in Figure 7. A nodal displacement was applied to three nodes at the vertices of the bottom surface of the laminate. As shown in Figure

7, node A was constrained in all the directions, node B was constrained in the x-direction and y-direction and free to expand or contract in the z-direction, while node C was only constrained in the y-direction while free to expand or contract in x and z-direction. The constraint of three nodes avoid the rotation of the laminate during the analysis. The longitudinal strains were taken at the middle surface of the adhesive layer, which is the average strain between the top and bottom of the adhesive ply. The transverse strains were also taken at the middle surface of the adhesive layer at a distance of $1\ mm$ from the adhesive gap mimicking the experimental tests. In the CCP specimens, residual strains within the adhesive layer can be categorized in three areas of interest: *stable region*, which is an area approximately $4\ mm$ away from the interface, the *adhesive gap region,* which is the $5\ mm$ distance between the cut plies, and the *interface* which is a location between the cut plies and the adhesive gap. Studies found in the literature on the CCP specimen do not provide specific requirement on the dimensions of the adhesive gap. A mesh convergence study was performed on the FE model with the same dimensions of the tested CCP laminate. The convergence study was performed for a mesh size of 8 mm, 4 mm, 2 mm, 1.3 mm, 1 mm, and 0.9 mm, as shown in Figure 6. The 1 mm mesh size with 20-node SOLID186 element was used for the analysis with quadratic displacement behavior generating 280908 element and 1987824 nodes, as shown in Figure 8.

As part of the FEM, the adhesive gap is in contact with the cut-ply laminates. In Ansys Workbench™ five different contact setting types are available: bonded, no separation, frictionless, rough, and frictional. Bonded and no separation belong to the linear contact type which considers that the contact area remains a constant, while frictionless, rough, and frictional, belong to the nonlinear contact type. Although nonlinear contact can model the true area of

contact during the application of the load, their nonlinearity aspect increases the computational time for the analysis. In addition, it can lead to convergence problems during the analysis. The first approach, considered by the authors, employed bonded contacts for all the surfaces at the interface of the cut-ply and the adhesive gap, in which no sliding or separation is allowed during the analysis. At a later stage of the research study, the contacts at the interface between cut plies and adhesive gap were modified to frictional in order to produce better correlation between the experimental and numerical results. The frictional contact, also known as “sticking”, does not allow the surfaces in contact to slide until a specific shear stress limit is exceeded [48].

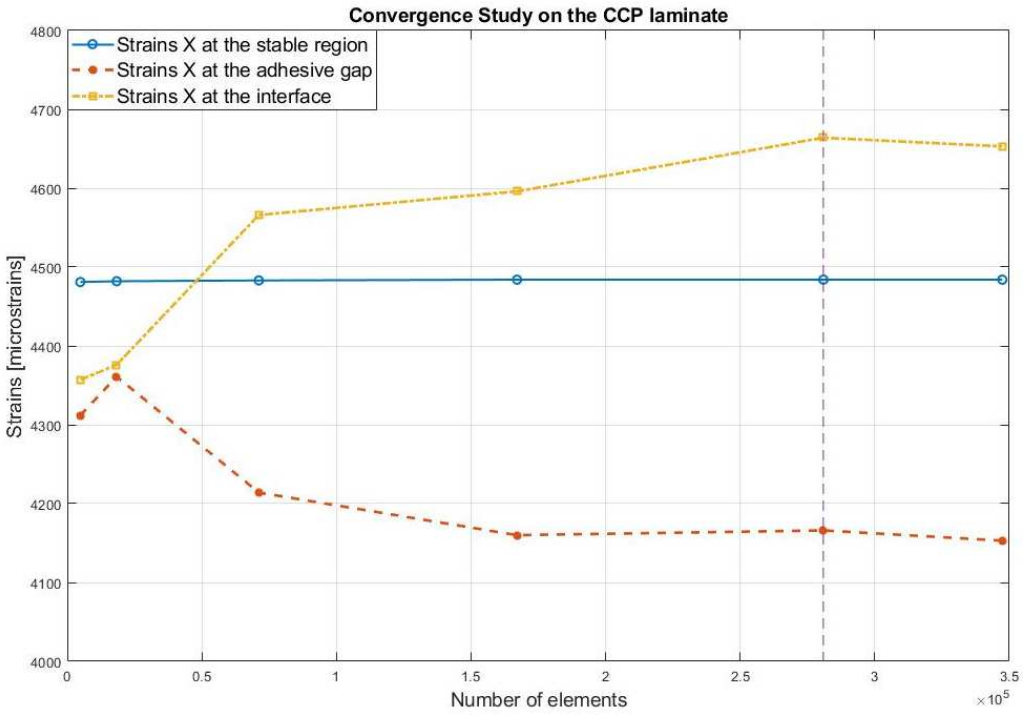

Figure 6. Mesh convergence study on the CCP laminate.

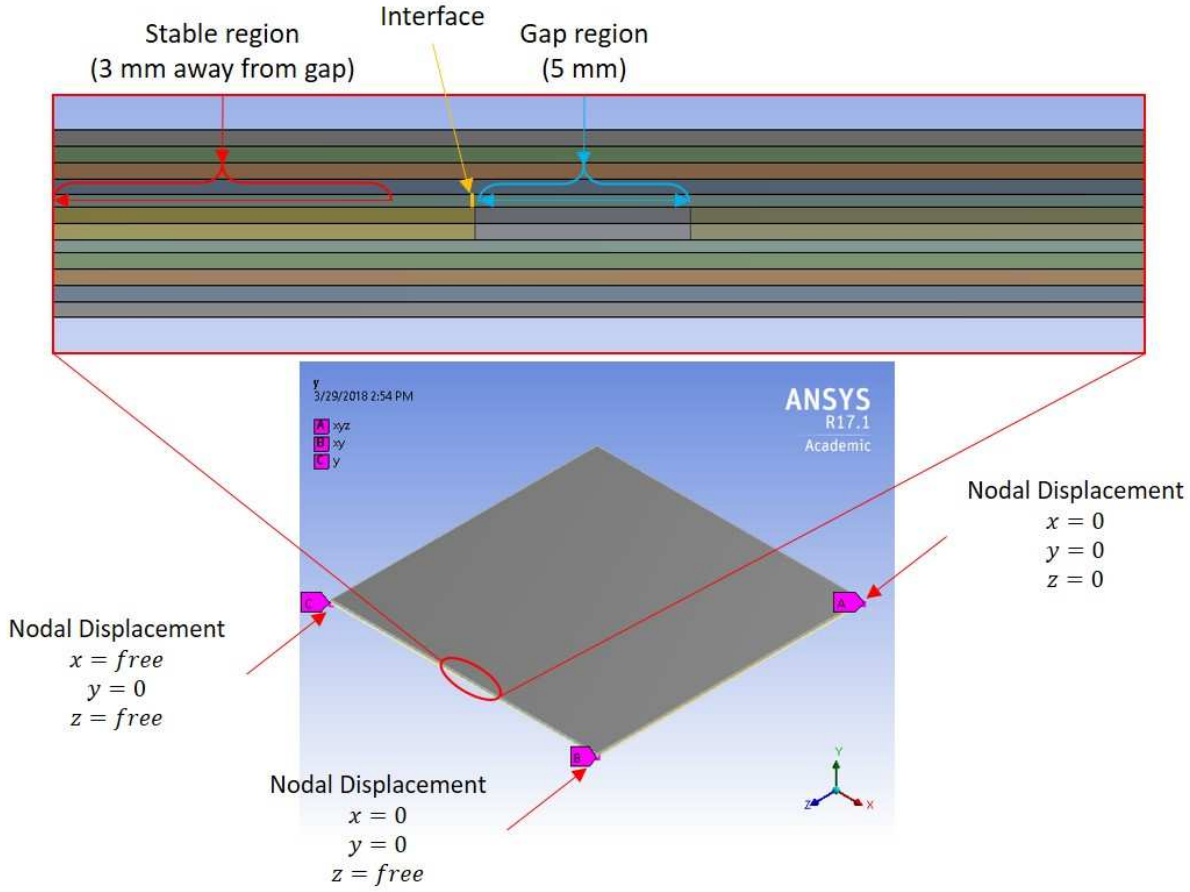

Figure 7. Boundary conditions on the CCP laminate.

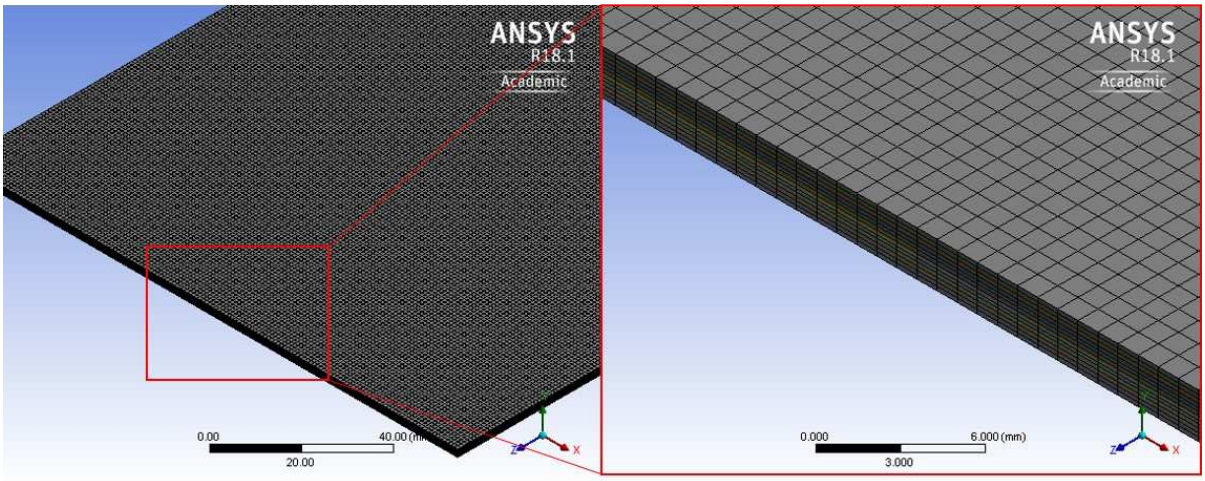

Figure 8. Mesh size (1 mm) on the entire CCP laminate.

It is important to note, that the numerical analysis does not account for chemical strains which arise during resin polymerization, as the finite element analysis software is unable to model cross-linking of polymers during a curing process. As such, the magnitude of the chemical strains obtained from the experimental tests, were added to the numerical results.

Results

The results obtained in this study have been divided into three sections: (i) Experimental results, (ii) FEA results, and (iii) residual stress determination. FEA was performed to confirm that the observed behavior in the experiments was consistent with the physical phenomenon included in the model. The experimental residual stresses were determined from the corresponding experimental residual strains assuming a linear elastic behavior of the resin, after which these results were compared to the Ansys Workbench™ model.

Experimental residual strains

The experimental strains were measured using the LUNA DSS fiber optic system. Figure 9(a) shows the total strain distribution for the unidirectional CCP laminate along the entire fiber length at each of the significant periods in time during the curing cycle. As shown in Figure 9(a), the transverse strain and longitudinal strains were found in between the highlighted peaks. The local pressure applied by the author prior the curing cycle was meant to partially identify the portion of the embedded sensor. The peaks shown in Figure 9, instead, are due to the polymerization of the resin at the edges of the laminate which provide an accurate estimation of the embedded fiber segment along the transverse or longitudinal direction of the CCP laminate. The data acquisition rate of the DSS allows the authors to detect many strain distributions along

the entire fiber for every portion of the curing cycle. As seen in Figure 9(a), after the heating phase ($Point\ \ B\ in$ **Figure 4**) the transverse strains are higher than the longitudinal strains, due to the higher CTE of carbon fiber along the transverse direction. As expected, before the polymerization of the resin, no additional strains arise inside the laminate during the curing phase between B and B'. One of the most crucial aspect of this study was to determine the right amount of chemical strains developed between B' and C, as this measured chemical strain was further added to the numerical model developed in this study. Although it was obvious the determination of the beginning of the cooling phase (point C) due to a visible drop in strains after opening the door of the oven, it was much harder to capture the moment in time when the resin started to polymerize. During the data analysis, the author observed that the polymerization reaction at the edge of the laminate created a strain peak as highlighted in Figure 9(a). In this manner, the beginning of resin polymerization was determined by observing changes in curvature at the edges of the laminate (magnified image in Figure 9(a)). In our study, the amount of chemical strains was determined to be approximately $120\ \mu\varepsilon$. This value of strains was determined from the difference in strain distribution, at both C and B' of the curing cycle, along the embedded section of the fiber.

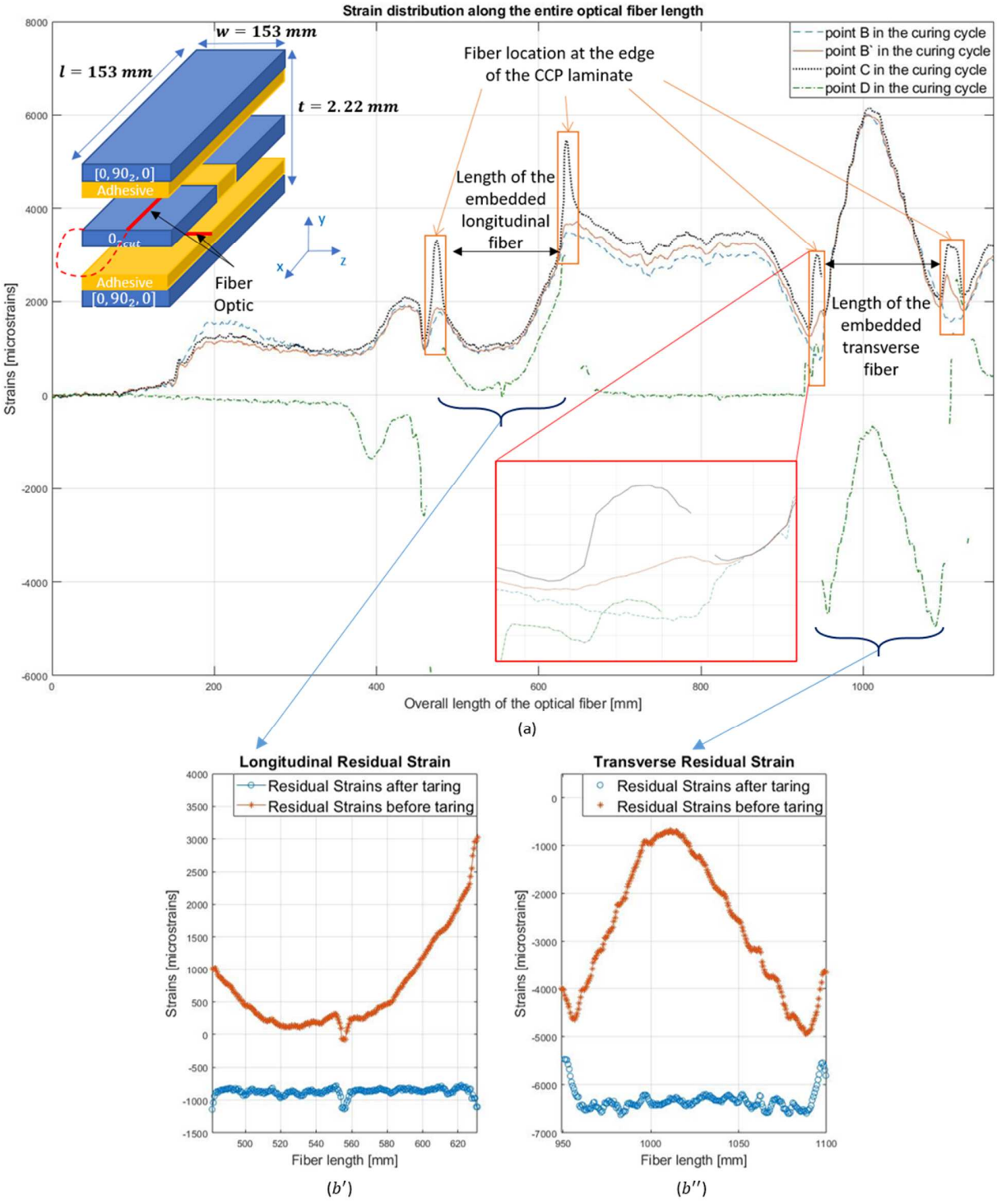

Figure 9: (a) Total strain distribution along the entire optical fiber length during all the three phases of the curing cycle for the Unidirectional CCP laminate; Strain distribution along the longitudinal (b') and transverse (b'') section of the optical fiber.

As shown in Figure 9(a), at point D of the curing cycle, the missing strain values (outside of the embedded fiber sections) are regions of the fiber which correspond to high strain gradients produced due to strain concentrations at the edges of the laminate. This high strain gradient is not captured by the DSS.

Three tests were performed for each configuration in order to guarantee the repeatability of the results. Residual strain distributions for both unidirectional and cross-ply CCP laminates are shown in Figure 10(a) as an average of the three tests. The repeatability among each of the three tests for each configuration was found to be within 5% of each other as measured by the DSS. However, it is important to note that the results shown in Figure 10(a), are representative of the residual strains shown in Equation 7, where the thermal, chemical and thermal expansion of the optical fiber have been accounted for. Thus, it is indicative that the contribution of the chemical and thermal expansion of the fiber account for approximately $120\ \mu\varepsilon$ and $1020\ \mu\varepsilon$ respectively. In addition, it is important to note that the contribution of the thermal strain for the CCP laminate are configuration, direction, and location dependent, such as the proximity to the adhesive gap. For the unidirectional CCP laminate, the longitudinal and transverse thermal strains of the adhesive are on average $880\ \mu\varepsilon$ and $4100\ \mu\varepsilon$, while for the cross-ply CCP laminate are approximately $1300\ \mu\varepsilon$ and $1750\ \mu\varepsilon$, respectively. The estimated average thermal strain was determined from edge to edge of the entire adhesive layer. However, the use of a single average thermal strain value was not employed in this study, as the DSS allowed the author to use point to point compensation. For this reason, the post-processing of the DSS was used to obtain the residual strains at the end of the cooling process by zeroing the strains at the end of the curing

phase (which neglected the contribution of the chemical and thermal expansion for the fiber), shown in Figure 9(b). The effect of the chemical strains and thermal expansion for the fiber was summed to the measured residual strains providing the strain distributions shown in Figure 10(a) and Figure 10(b).

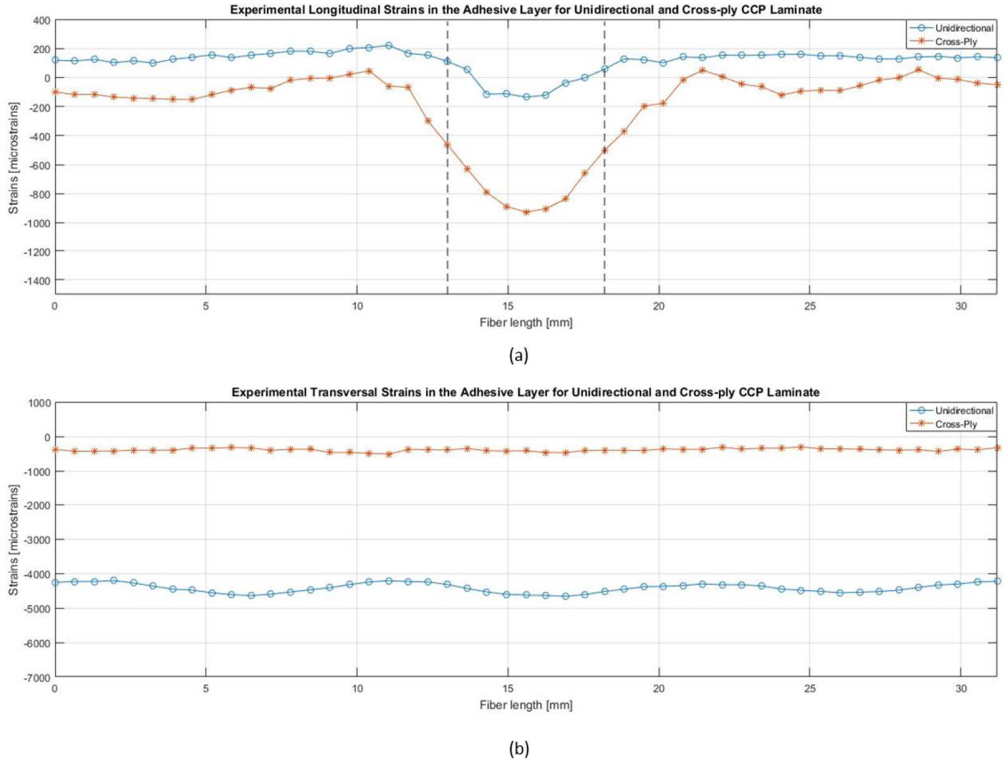

Figure 10. (a) Longitudinal strains and (b) transverse strain distribution within the adhesive layer for unidirectional and cross-ply laminates obtained though experimental tests.

In the unidirectional CCP laminate, tensile longitudinal residual strains were observed as shown in Figure 10(a). The experimental results showed a plateau of the longitudinal strain field at approximately $127\ \mu\varepsilon$ in the stable region of the adhesive layer. As we approach the interface between the cut layers and the adhesive gap (which is comprised between the vertical dashed lines in Figure 10(a)), the strains slightly increase up to $220\ \mu\varepsilon$ before gradually decreasing to a

compressive value reaching a minimum of -135 με right at the center of the adhesive gap. As it can be seen in Figure 10(b), compressive transverse residual strains were observed after the cooling phase, which fluctuated between -4638 με and -4204 με with an average of -4421 με.

For the CCP cross-ply laminate, conversely, compressive longitudinal residual strains were observed in the stable region of the adhesive layer reaching a plateau of -75 με as shown in Figure 10(a). Similar to the strain distribution observed in the unidirectional case, a strain increment was also observed in the cross-ply configuration as we approach the adhesive gap. However, in these conditions the reduction of strain was more pronounced, reaching a value of -926 με. Compressive transverse residual strains in the cross-ply configuration showed a constant strain distribution with strain values that oscillate between -410 με and -372 με with an average of -391 με

Numerical residual strains

Finite Element Methods (FEM) was employed to obtain residual strain distributions in the adhesive layer for both configuration of the CCP laminate.

As previously described in the methodology section, the FEM was developed with different contact settings between the adhesive gap and the cut plies. The following sections highlights the different results obtained based on the appropriate contact method.

Figure 11(a) shows longitudinal strains distributions for the unidirectional CCP laminate modeled with bonded and frictional contact settings for the faces that connect the cut plies to the adhesive gap. These results were further compared to the experimental findings. In a first step, the CCP laminate was modeled with face-to-face bonded contacts for all the layers. As can be seen in

Figure 11(a), bonded contacts showed longitudinal strain values of 139 με at the stable region of the adhesive layer. Although this type of contact settings provided similar results in this region, it created a strain distribution at the interface and within the adhesive gap that were in contrast with those observed experimentally. In fact, bonded contact showed compressive longitudinal strains of -44 με at the interface and tensile longitudinal strains of 132 με within the adhesive gap, which disagreed with the experimental results. For this reason, the face-to-face contact settings between the cut plies and the adhesive gap were modified from bonded to frictional. The friction coefficient used for the FE analysis was 0.5. However, the analysis was performed varying the friction coefficient from 0.3 to 0.7 showing variations on the strain distributions less than 0.1%. It is important to note that the stable region, is not affected by the two analyzed contact setting. Tensile longitudinal strains of 142 με were observed in the stable region of the adhesive layer. However, tensile longitudinal strains of 595 με and compressive longitudinal strains of -757 με were observed at the interface and within the adhesive gap, respectively. Although the frictional contact setting provided the same strain distribution as the experimental tests, the magnitude of the longitudinal strains at the interface and within the adhesive gap are four times higher than the experimental findings. The elastic modulus of the adhesive gap was modified to 0.493 Gpa obtained through the rule of mixture considering the absence of the carrier within the gap region. Longitudinal strains of 142 με, 230 με, and -190 με were observed in the stable region, interface, and adhesive gap respectively, for the updated stiffness as shown in Figure 11(b). As seen in Figure 11(b), the optimal contact setting that reproduced our experimental findings consist of a frictional contact between the cut-plies and the adhesive gap. As such, all further FE models in this study made use of such type of contact setting.

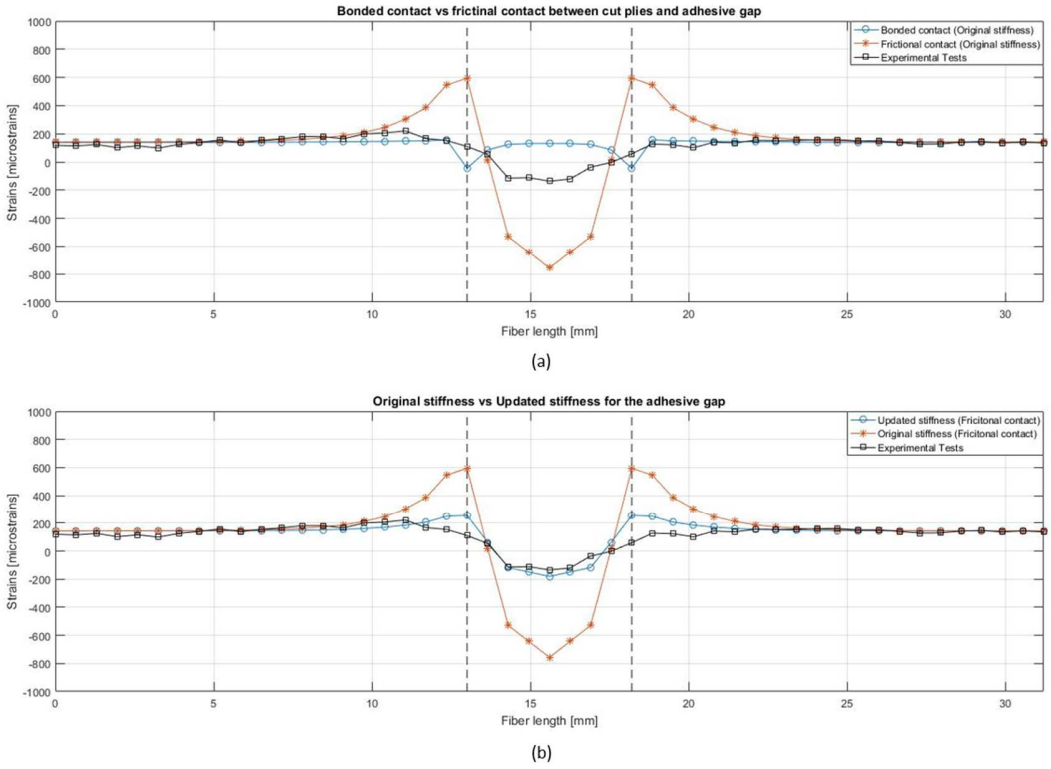

Figure 11. (a) Unidirectional CCP laminate modeled with bonded and frictional contacts; (b) Unidirectional CCP laminate modeled the change in stiffness within the adhesive gap.

Figure 12 shows the location of the midplane longitudinal and transverse strains in Ansys Workbench™ model. The FEA used the Classical Lamination Theory (CLT) to compute the strain distribution along the adhesive layer. As can be seen from Figure 12, the magnitude of the longitudinal strains for the unidirectional and cross-ply CCP laminate reached a maximum value of approximately $4700\ \mu\varepsilon$ and $4300\ \mu\varepsilon$, respectively. The thermal and chemical effect were removed from the previous strains, providing the strain distributions shown in Figure 13(a) and Figure 14(a). In the FEM the thermal contribution is given by the product of CTE of the adhesive and the ΔT that the laminate experienced during the curing process, while the chemical strain values were obtained experimentally through the use of the DSS.

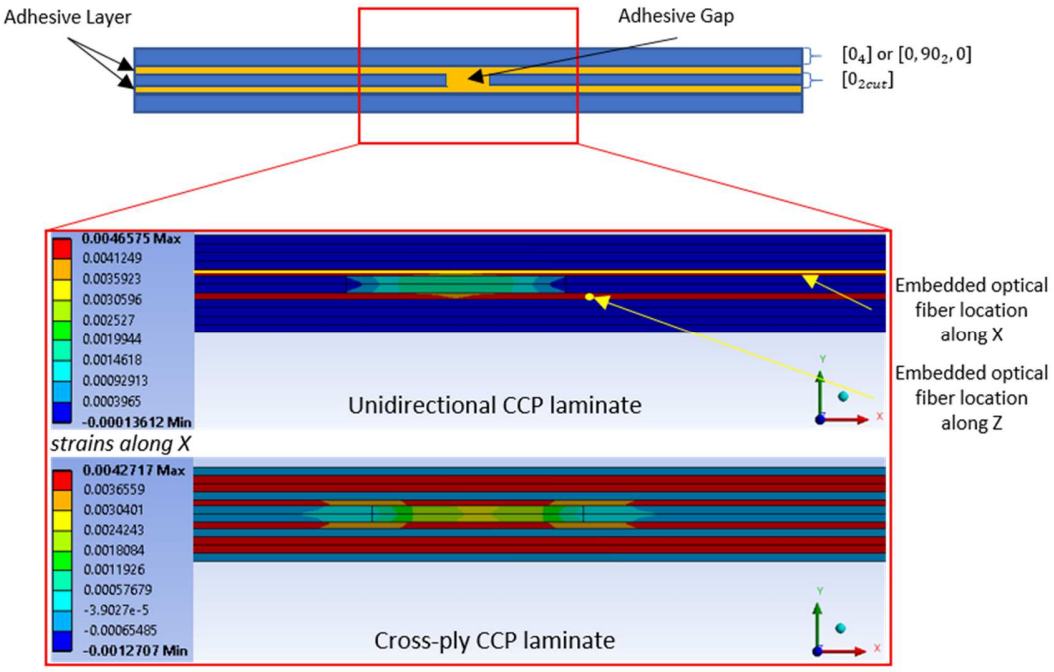

Figure 12. FEA results of longitudinal and transverse strains in the adhesive layer for the unidirectional laminate.

Figure 13 and Figure 14 showed the comparison between experimental results and FEA on the longitudinal strains and transverse strain distribution within the adhesive layer for unidirectional CCP laminate (Figure 13) and cross-ply (Figure 14) CCP laminate. In case of the unidirectional CCP laminate, the FE model showed tensile longitudinal residual strains in the stable region reaching a tensile value of $142\ \mu\varepsilon$, increasing up to $257\ \mu\varepsilon$ before dropping to a compressive value of $-182\ \mu\varepsilon$ within the adhesive gap. The transverse residual strains showed a constant value of $-4300\ \mu\varepsilon$.

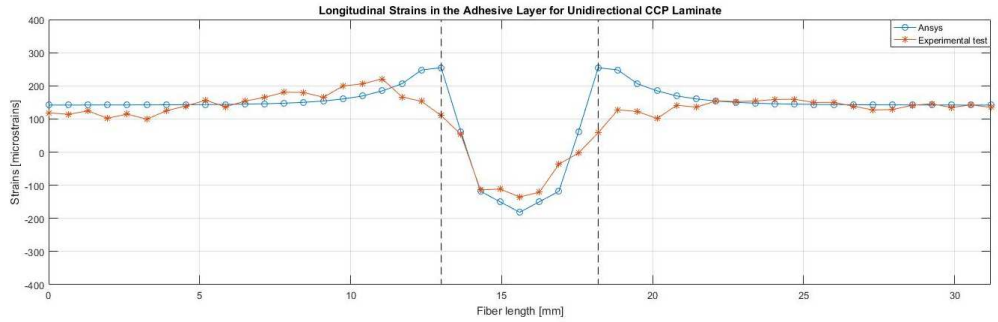

(a)

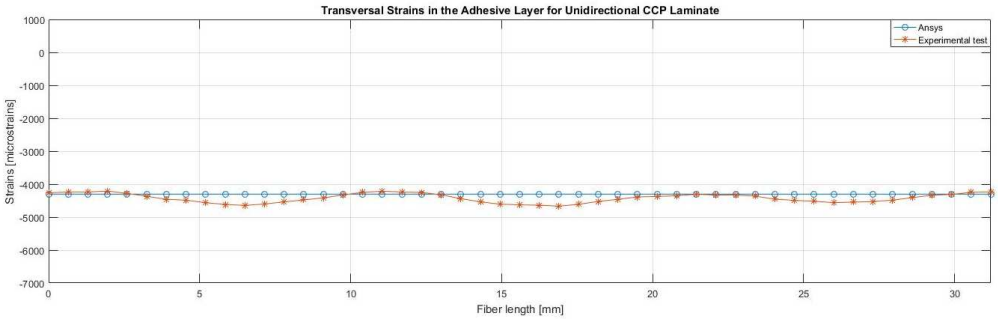

(b)

Figure 13. Comparison between Experimental test and Numerical Analysis on the longitudinal strains (a) and transverse strain (b) distribution within the adhesive layer for unidirectional laminates.

For the cross-ply CCP laminate, the strains converged to a constant value of -95 με in the stable region as shown in Figure 14 (a). As the sensing fiber approaches the adhesive gap the strains gradually decrease reaching a compressive value of -963 με. The transverse residual strains showed a constant value of -335 με.

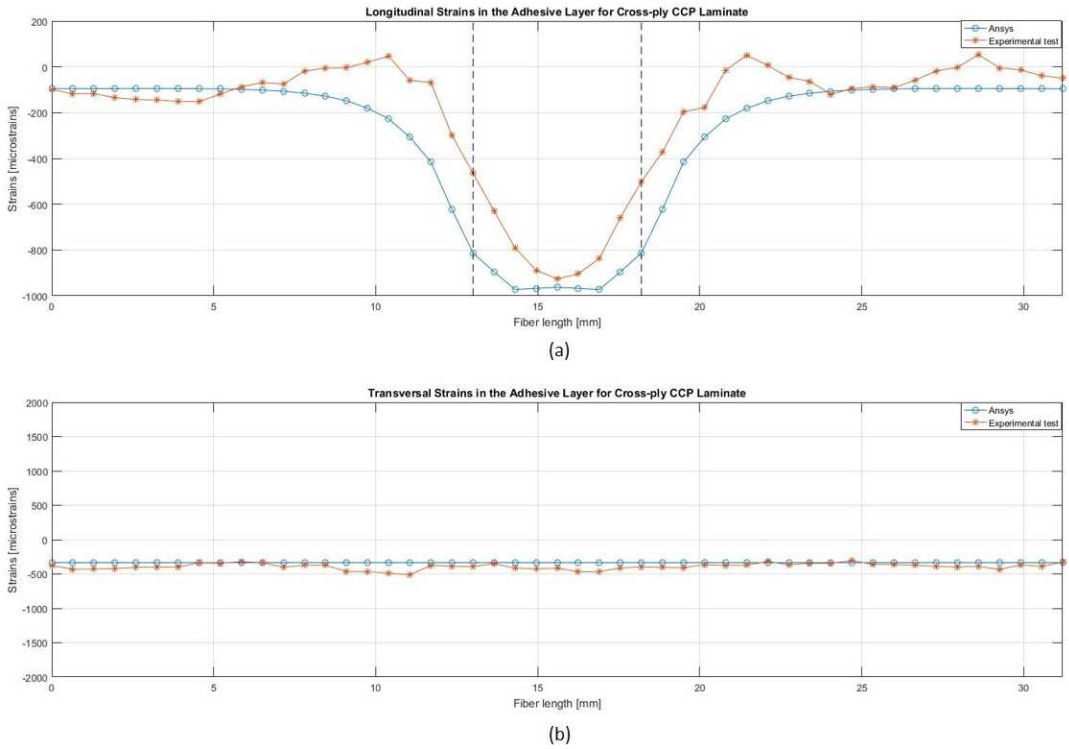

Figure 14. Comparison between Experimental test and Numerical Analysis on the longitudinal strains (a) and transverse strain (b) distribution within the adhesive layer for cross-ply laminates.

Both unidirectional and cross-ply configurations showed similar behavior with higher residual strains for the cross-ply in comparison to the unidirectional case, as shown in Figure 13 and Figure 14. A sensitivity study was performed by considering an uncertainty of ±10% on the mechanical and thermal properties of the adhesive. The study demonstrated that the un certainty did not have a significant impact on the final residual stress results.

Residual Stress Determination

Residual stresses were computed from the corresponding residual strains through linear elastic analysis. Figure 15 and Figure 16 show the residual stress formation in the adhesive layer during

the cooling process for the unidirectional and cross-ply configuration, respectively. The two configurations show tensile residual stresses for both CCP laminates. As expected, the cross-ply produced higher residual longitudinal and transverse stresses than the unidirectional. At the end of the cooling phase, experimental tests showed approximate longitudinal and transverse residual stresses for the unidirectional CCP laminate of $8.6\ MPa$ and $2.2\ MPa$, respectively. These results are in good agreement with FE model which showed longitudinal and transverse stresses of $8.6\ MPa$ and $2.5\ MPa$, thus generating a percentage difference of less than 1% for the longitudinal stresses and approximately 14% for the transverse stresses. Experimental tests on cross-ply CCP laminates showed longitudinal and transverse residual stresses of $9.9\ MPa$ and $9.7\ MPa$, respectively, matching those from the FE model of $10.2\ MPa$ and $9.7\ MPa$. In this scenario the percentage difference was computed to be 3% for the longitudinal stresses and less than 1% for the transverse stresses. Considering the measured residual stresses from the adhesive strength ($14.3\ MPa$), the amount of longitudinal and transverse residual stresses in the stable region for the unidirectional CCP laminate are 61% and 19% of the total strength of the adhesive, while for the cross-ply CCP laminate are 72% and 71%, respectively.

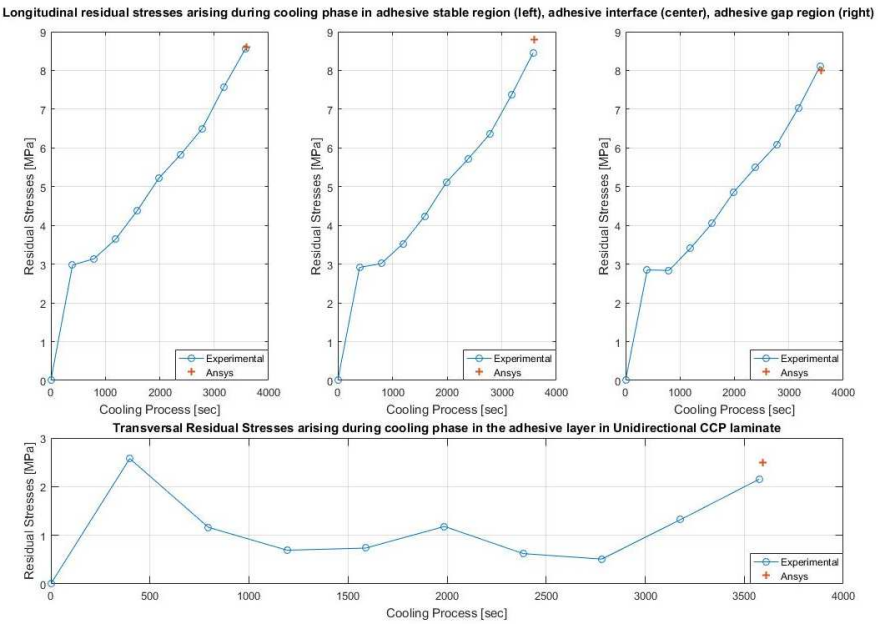

Figure 15. Longitudinal residual stresses in the three regions (top) and transverse residual stresses (bottom) within the adhesive layer arising during cooling process for Unidirectional CCP laminate.

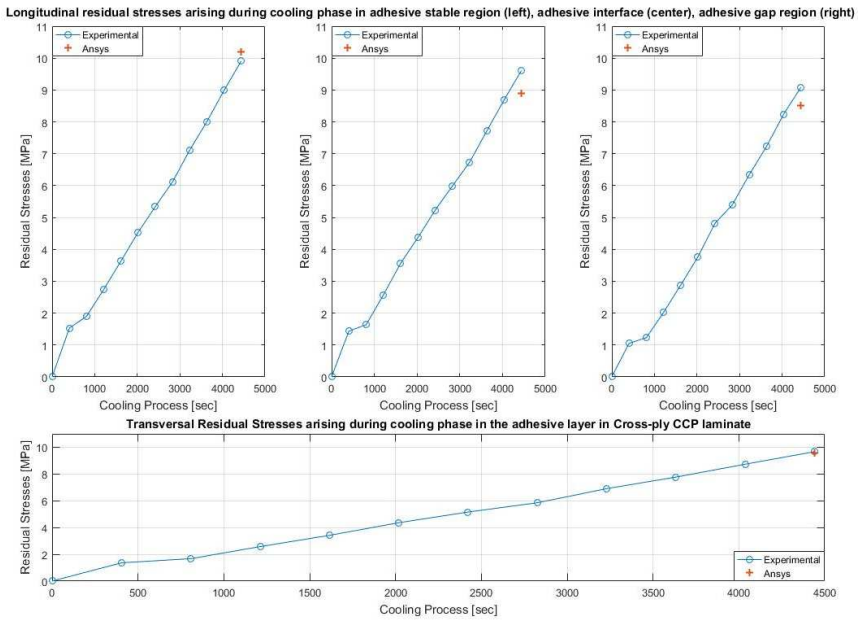

Figure 16. Longitudinal residual stresses in the three regions (top) and transverse residual stresses (bottom) arising during cooling process for Unidirectional CCP laminate.

Figure 17 shows the tri-axial stress state at the stable region of the adhesive layer obtained through the FE model. Although both unidirectional and cross-ply configurations exhibit significant longitudinal and transverse residual stress values, through-thickness and shear stresses are observed to be negligible as obtained from the FE model. The highest shear stresses were observed in the *x-y* plane of the cross-ply CCP laminate which are two order of magnitude lower than the normal stresses along the in-plane direction.

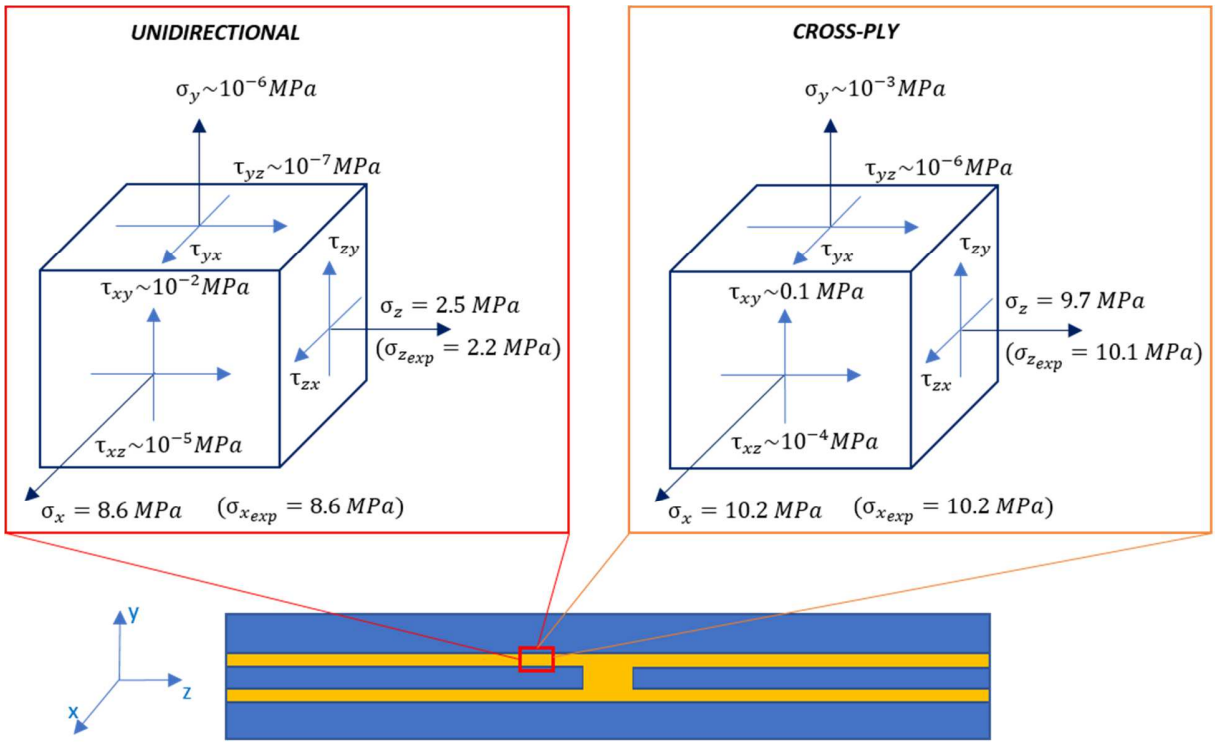

Figure 17. Tri-axial stress state at the stable region of the adhesive layer for both Unidirectional and cross-ply CCP laminate obtained through FE analysis.

Discussion

Another crucial aspect of the experimental tests was measuring the amount of chemical strains arising during the curing phase after resin polymerization. The amount of the measured chemical strains was added to the FE model which does not account for cross-linking effects within the resin. Although the gel time of a resin is provided by the manufacturer, it is difficult to know the exact time of the beginning of the polymerization reaction through the DSS. In fact, prior to the cooling phase, the recorded total strains captured by the DSS, is comprised of thermal (order of 10^3) and chemical (order of 10^2) strains. Since thermal component is one order of magnitude larger than the chemical strains, small fluctuation in temperature ($\pm 1^o C$) have a larger effect on the thermal in comparison to the chemical strains. However, the authors were able to isolate and capture the moment at which the polymerization of the resin occurred by monitoring changes of strain distributions at the edges of the laminate. Although both sections of the embedded optical fiber experienced cross-linking effect due to the polymerization reaction, this phenomenon was more visible at transverse section of the embedded fiber.

The experimental results allowed the authors to validate and correlate the FE model with an understanding of the physicals phenomenon at play. An initial FE model considering bonded contacts at the interface between the gap and the cut-plies resulted in opposite strain distribution within the adhesive gap as those obtained from the DSS. As such, a comparison to experimental results, the authors were able to recognize that bonded contacts in the FE model did not recreate the manufactured CCP laminate configuration in this study. The first reason, is that the FE model of the CCP laminate has a perfect cut between the cut-plies and adhesive gap,

while in reality the cut plies are manufactured through hand lay-up sequence in which the edges of the carbon fiber layers are not uniformly cut. Secondly, during the curing phase, the resin is viscous enough to flow within the gap. When the glass transition temperature is reached, the resin start polymerizing within the adhesive gap and all around the edges of the cut plies. This type of behavior at the interface of the adhesive gap, was mimicked using a frictional contact setting in ANSYS Workbench™. In addition, it was important to consider the lack of a nylon carrier within the adhesive gap which lowered the stiffness in that region of the CCP. After updating the elastic modulus for the adhesive gap through the rule of mixture to the value of 0.493 GPa, the FE analysis showed the same order of magnitude for the longitudinal strains as the experimental results. In summary it was found that a frictional contact setting produced a realistic behavior for strain distribution at the interface while the updated stiffness for the adhesive gap provided the right magnitude of those strains.

As can be seen in Figure 13(a), the FEA was able to mimic the longitudinal strain distribution along the stable region of the adhesive layer as well as the adhesive gap. The FE model was also able to capture the strain peaks at the interface which were barely observed by DSS. In fact, the residual strain values near the interface on the left-hand side of the CCP laminate are approximately $221\ \mu\varepsilon$ compared to the ones on the right-hand side which are approximately $101\ \mu\varepsilon$. The difference in the location of the interface between the FE model and the experimental CCP laminate is due to variations during the manufacturing process of the CCP laminate. In addition, the variation in adhesive gap size and location translates to the formation and location of strain peaks which shows up in the FE model but not in the DSS experimental results (Figure 14(a)). As previously mentioned the strain distribution along the optical fiber is

averaged at every 1.3 mm throughout the length of the fiber. As such, high strain gradients are not captured by the DSS system. Another phenomenon observed in Figure 13(b) is the fluctuation of the transverse strains (of approximately 400 $\mu\varepsilon$) due to the transverse shrinkage of the unidirectional CCP laminate. In fact, applied load transverse to the carbon fiber direction is supported by the adhesive, which produces a non-constant behavior. The same phenomenon was observed when determining the transverse Young's modulus of the carbon fiber during a pull test. In this scenario, the optical fiber was attached to the surface of the specimen, transverse to the carbon fiber direction, resulting in strain measurements showing the same fluctuating strain distribution.

Experimental longitudinal strain distribution in the cross-ply CCP laminate exhibits peaks at both sides of the adhesive gap which were not observed in the FE model, shown in Figure 14(b). This is probably due to the fact that resin polymerization does not occur instantly throughout the entire volume of the adhesive layer creating a slightly different strain distribution between the two sides of the CCP laminate. Longitudinal strain distribution computed by the FE model showed the same values in the stable region of the adhesive layer as the experimental results. However, the results show higher discrepancy within the adhesive gap compared to the unidirectional case, as shown in Figure 14(a). This is due to the aforementioned phenomenon of the resin polymerization process, which cannot be fully controlled over the entire adhesive layer. Transverse strains in the cross-ply CCP laminate do not experience the fluctuation observed in the unidirectional case since the adhesive layer does not experience contraction during the cooling phase (Figure 14(b)).

It is important to note that the FE model is unable to match the entire stress determination throughout the entire curing cycle, as such validation only occurs at the end of the cooling process. However, the experimental results show a transient stress determination ending at the same state as that predicted by Ansys Workbench™. As shown in Figure 15 and Figure 16, longitudinal stresses in both unidirectional and cross-ply laminate are linear with the exception of a small deflection at the beginning of the cooling phase. In fact, at the end of the curing phase the CCP laminate was cooled down to room temperature by opening the door of the oven. As such, the temperature experienced a rapid drop before stabilizing and decreasing linearly which generates the small deviation observed in both of the CCP configurations. For the case of the cross-ply CCP laminate, the tensile longitudinal and transverse residual stress distributions increased linearly during the entire cooling process, as shown in Figure 15. For the unidirectional CCP laminate, the longitudinal residual stresses showed the same behavior as the cross-ply case. The transverse residual stresses exhibit non-linear behavior for the first part of the cooling phase before stabilizing to a linear trend at the end of the cooling cycle, as shown in Figure 16. This stress behavior is due to the contraction of the embedded fiber optic. As mentioned in the experimental setup section of this manuscript, thermal strains due to the expansion or contraction of the optical fiber had to be considered. While the optical fiber is free to expand during the heating phase, it becomes an integral part of the laminate after the glass transition point due to resin polymerization. Therefore, in the cross-ply CCP laminate all the layers are constrained to each other. The optical fiber embedded longitudinally and transverse ly within the adhesive layer does not shrink to the original dimension after the cooling phase. On the other hand, the embedded optical fiber in the unidirectional CCP laminate, exhibits two different

behaviors. The longitudinally embedded fiber in the adhesive layer does not contract during the cooling phase because of the quasi-zero CTE along the fiber direction of the neighboring carbon fiber layer. However, because the CTE of the adhesive layer is the same as the transverse CTE of the carbon fiber layer, the embedded optical fiber shrinks as much as the adhesive layer. As the authors were interested in capturing the residual stress formations at the end of the cooling phase, the total additional thermal strains from the polyimide fiber were removed at the beginning of the cooling phase (point C shown in Figure 4).

Conclusion

This study demonstrated the presence of longitudinal and transverse residual stresses in the adhesive layer of a CCP laminate for both the unidirectional and cross-ply configurations during the curing process. The results showed that the cross-ply configuration provided higher longitudinal and transverse residual stresses compared to the unidirectional configuration, which translates into a higher strength degradation of the adhesive layer. The FE analysis on the CCP laminate showed the frictional contact behavior at the interface between the cut plies and the adhesive gap was necessary to match the experimentally obtained strain distribution. The validation of the FE model against the experimental results will allow, in the future, to assess the impact of those parameters, such as curing temperature, mechanical and thermal properties of the neighboring carbon fiber layers as well as the adhesive layer, on residual stress formation in CCP laminates. In addition, the tensile nature of the residual stresses is expected to be detrimental on the crack growth rate for mode II fatigue study, promoting the disbond

propagation in the direction of these stresses. Finally, the experimental results were in good agreement with the numerical model showing a maximum discrepancy of approximately 3% within a stable region.

Acknowledgement

The authors kindly acknowledge the support of NVIDIA Corporation and their donation of a TESLA K40 and Quadro P6000 GPU hardware card to the Holistic Structural Integrity Process Laboratory at Clarkson University.

References

[1] K. B. Katnam, L. F. Da Silva and T. M. Young, "Bonded Repair of Composite Aircraft Structures: A Review of Scientific Challenges and Opportunities," *Progress in Aerospace Sciences,* pp. 26-42, 2013.

[2] T. Kruse, T. Körwien, R. Ruzek, R. Hangx and C. Rans, "Fatigue behaviour and damage tolerant design of bonded joints for aerospace application on Fibre Metal Laminates and composites," in *29th Symposium of the International Committee on Aeronautical Fatigue (ICAF 2017)*, Nagoya, Japan, 2017.

[3] R. Sachse, M. Käß, A. K. Pickett and P. Middendorf, "Numerical Simulation of Fatigue Crack Growth in the Adhesve Bondline of Hybrid CFRP Joints," in *COMPOSITES 2015*, Bristol, 2015.

[4] R. Sachse, A. K. Pickett, W. Adebahr, M. Klein, M. Käß and P. Middendorf, "Experimental investigation of mechanical fasteners regarding their influence on crack growth in adhesively bonded CRFP-joints subjected to fatigue Loading," in *20th International Conference on Composite Materials, ICCM20*, Copenhagen, 2015.

[5] T. Kruse , T. Körwien, S. Heckner and M. Geistbeck, "Bonding of cfrp primary aerospace structures – crackstopping in composite bonded joints under fatigue," in *20th International Conference on Composite Materials, ICCM 20*, Copenhagen, 2015.

[6] C. Gonzales, "Machine Design," Informa, 29 06 2015. [Online]. Available: https://www.machinedesign.com/fasteners/lighter-fasteners-and-adhesives-boost-aircraft-efficiency. [Accessed 12 09 2018].

[7] M. J. Piehl , R. H. Bossi and K. Y. Blohowiak, "Efficient certification of bonded primary structure," in *International SAMPE Technical Conference*, 2013.

[8] F. A. A. (FAA), "COMPOSITE AIRCRAFT STRUCTURE," U.S. Department of Transportation, Oklahoma City, OK , 2009.

[9] A. Skorupa and M. Skorupa , Riveted Lap Joints in Aircraft Fuselage: Design, Analysis and Properties, Springer Science, 2012.

[10] M. Davis and D. Bond, "Principles and practices of adhesive bonded structural joints and repairs," *Adhesion and adhesives,* pp. 91-105, 1999.

[11] M. M. Shokrieh and A. R. Ghanei Mohammadi, "the importance of measuring residual stresses in composite materials," in *Residual Stresses in composite materials*, Woodhead Publishing, 2014, pp. 3-12.

[12] D. R. Daverschot, A. Vlot and H. J. Woerden, "Thermal Residual Stresses in Bonded Repairs," *Applied Composite Material,* pp. 179-197, 2002.

[13] A. M. Albat, D. P. Romilly and M. D. Raizenne, "Thermal Residual Stresses in Bonded Composite Repairs on Cracked Metal Structures," *Materials Technology,* pp. 299-308, 2000.

[14] R. A. Bartholomeusz, A. A. Baker, R. J. Chester and A. Searl, "Bonded Joints with Through-Thickness Adhesive Stresses - Reinforcing the F/A-18 Y470.5 Bulkhead," *Adhesion & Adhesives,* pp. 173-180, 1999.

[15] L. J. Hart-Smith, "analysis and design of advanced composite bonded joints," NASA CR-2218, 1974.

[16] G. A. Schoeppner, D. H. Mollenhauer and E. V. Iarve, "PREDICTION AND MEASUREMENT OF RESIDUAL STRAINS FOR A COMPOSITE BONDED JOINT," *Mechanics of Composite Materials,* vol. Vol. 40, pp. 187-210, 2004.

[17] G. A. Schoeppner, D. Mollenhauer, K. B. Bowman and E. Iarve, "Residual stress prediction and measurement in composite bonded joint adhesive," in *proceedings of the third Australasian Congress on Applied Mechanics*, Sydney, 2002.

[18] L. Aminallah, T. Achour, B. Bachir Bouiadjra, B. Serier, A. Amrouche, X. Feaugas and N. Benssediq, "Analysis of the distribution of thermal residual stresses in bonded composite repair of metallic aircraft structures," *Computational Materials Science 46,* pp. 1023-1027, 2009.

[19] R. Mhamdia, B. Bachir Bouiadjra, B. Serier and M. Belhouari, "The Effect of Thermal Residual Stresses on the Performances of Bonded Composite Repairs in Aircraft Structures," in *Proceedings of the 2012 International Conference on Industrial Engineering and Operations Management*, Instanbul, 2012.

[20] C. D. Rans and R. C. Alderliesten, "Damage Tolerance Philosophy for Bonded Aircraft Structures," in *Proceedings of the 25th Symposium of the International Committee on Aeronautical Fatigue*, Rotterdam, 2009.

[21] R. Marissen, *Fatigue Crack Growth in ARALL, A hybrid Aluminium-Aramid Composite Material, crack growth mechanisms and quantitative predictions of the crack growth rate,* Delft University of Technology, 1988.

[22] F. N. Ribeiro, M. Marcias and C. D. Rans, "Evaluation of mode II fatigue disbonding using Central Cut Plies specimen and distributed strain sensing technology," The journal of adhesion, 2018.

[23] G. Allegri, M. I. Jones, M. R. Wisnom and S. R. Hallet, "A New Semi-Empirical Model for Stress Ratio Effect on Mode II Fatigue Delamination Growth," *Composites Part A: Applied Science and Manufacturing Volume 42,* pp. 733-740, 2011.

[24] J. G. William, "On the calculation of energy relaease rates for cracked laminates," *International Journal of Fracture,* pp. 101-119, 1988.

[25] L. A. Carlsson, J. W. Gillespie and R. B. Pipes, "On the analysis and design of the End Notched Flexure (ENF) specimen for mode II testing," *Journal of composite materials,* pp. 594-604, 1986.

[26] G. C. Tsai, "Composite ENF specimens and conduct three-point test to calculate mode II fracture toughness," *9th International conference of engineering education,* 2006.

[27] H. Wang and T. Vu-Khanh, "Use of End Loaded Split (ELS) test to study stabe fracture behavior of composite under mode II loading," *Composite structures,* pp. 71-79, 1996.

[28] R. H. Martin and B. D. Davidson, "Mode II fracture toughness evaluation using four point bending end notched flexure test," *Composite science and technology,* pp. 251-256, 1992.

[29] C. Schuecker and B. D. Davidson, "Effect of friction on the perceived mode II delamination toughness from three and four poinit bending end notched flexure test," *Composite structures: theory and practise,* pp. 334-344, 2001.

[30] A. P. f. C. M. APCM, "DA4518 Epoxy Prepreg System," 50 09 2018. [Online]. Available: http://www.prepregs.com/da-4518/. [Accessed 15 12 2018].

[31] ASTM International, "Standard Test Method for Tensile Properties of Polymer Matrix Composite Materials," West Conshohocken (PA), 2017.

[32] ASTM International, "Standard Test Method for Through-Thickness “Flatwise” Tensile Strength and Elastic Modulus of a Fiber-Reinforced Polymer Matrix Composite Material," West Conshohocken (PA), 2015.

[33] ASTM International, "Standard Test Method for Shear Properties of Composite Materials by the V-Notched Beam Method," West Conshohocken (PA), 2012.

[34] A. International, "Standard test method for tensile properties of plastic," West Conshohocken (PA), 2002.

[35] L. Inc., "LUNA defying impossible," 02 02 2017. [Online]. Available: https://lunainc.com/wp-content/uploads/2016/07/ODB5_DataSheet_Rev13_020217.pdf. [Accessed 28 01 2019].

[36] Correlated Solutions, "VIC-2D Reference Manual," Correlated Solutions, 2016.

[37] HBM, "Strain Gauge | Stress Gauge | Accessories | HBM," HBM strain gauges, , 16 01 2016. [Online]. Available: https://www.hbm.com/en/0014/strain-gauges/. [Accessed 23 09 2018].

[38] F. Xin, S. Changsen, Z. Xiaotan and A. Farhad , "Determination of the coefficient of thermal expansion with embedded long-gauge fiber optic sensors," *Measurement Science and Technology,* pp. 1-8, 2009.

[39] L. F. da Silva and R. D. Adams, "Measurement of the mechanical properties of a carbon reinforced bismaleimide over a wide range of temperatures," *Mecanica Experimental,* pp. Vol 14, 29-34, 2007.

[40] Y.-L. Lo and H.-S. Chuang, "Measurement of thermal expansion coefficients using an in-fibre Bragg-grating sensor," *Measurement Science and Technology,* pp. 1543-1547, 1998.

[41] A. D. Kersey, M. A. Davis, H. J. Patrick, M. LeBlanc, K. P. Koo, C. G. Askins, M. A. Putnam and E. J. Friebele, "Fiber Grating Sensors," *Journal of Lightwave Technology,* pp. Vol.15, No.8, 1997.

[42] LUNA, "Distributed Fiber Optic Sensing: Temperature Compensation of Strain Measurement," Luna Innovations Incorporated, Roanoke (VA), 2013.

[43] MatWeb, "Aluminum6061-T6," MatWeb material property data, 19 10 2007. [Online]. Available: http://www.matweb.com/search/DataSheet.aspx?MatGUID=b8d536e0b9b54bd7b69e4124d8f1d20a&ckck=1. [Accessed 02 05 2017].

[44] MatWeb, "Aluminum6063-T6," MatWeb material property data, 19 10 2007. [Online]. Available: http://www.matweb.com/search/DataSheet.aspx?MatGUID=333b3a557aeb49b2b17266558e5d0dc0. [Accessed 02 05 2017].

[45] A. P. C. M. APCM, "DA 4518 Epoxy Prepreg System," [Online]. Available: http://www.prepregs.com/wp-content/uploads/2016/06/4518regular.pdf. [Accessed 05 02 2019].

[46] A. P. C. M. APCM, "DA 4518U Unidirectional Carbon Epoxy Prepreg System," [Online]. Available: http://www.prepregs.com/wp-content/uploads/2016/06/4518ucarbondatasheet.pdf. [Accessed 05 02 2019].

[47] I. I. Poly-Tech, "Poly-Tech Industrial, Inc.," 19 03 2011. [Online]. Available: https://www.polytechindustrial.com/products/plastic-stock-shapes/nylon-66. [Accessed 28 10 2017].

[48] Ansys, *Ansys Help viewer,* 2017.

[49] M. A. Sohail Khana, F. Benyahiaa, B. Bachir Bouiadjra and A. Albedah, "Analysis and Repair of Crack Growth Emanating from V-Notch under Stepped Variable Fatigue Loading," in *XVII International Colloquium on Mechanical Fatigue of Metals (ICMFM17)*, 2014.

[50] H. Hosseini-Toudeshky, "Effects of composite patches on fatigue crack propagation of single-side repaired aluminum panels," *Composite Structures,* pp. 243-251, 2006.

[51] H. Aglan, Q. Y. Wang and M. Kehoe, "Fatigue behavior of bonded composite repairs," *Journal of Adhesion Science and Technology,* pp. 1621-1634, 2002.